Pergamon

PII: S0021-9169(96)00062-1

Journal of Atmospheric and Solar-Terrestrial Physics, Vol. 59, No. 8, pp. 873–890, 1997

1364-6826/97 $17.00+0.00

Co-ordinated studies using imaging riometer and incoherent scatter radar

P. N. Collis* and J. K. Hargreaves

Engineering Department, University of Lancaster, Bailrigg, Lancaster LA1 4YQ, U.K.

(*Received in final form* 4 *March* 1996; *accepted* 21 *March* 1996)

Abstract—A 49 beam imaging riometer (IRIS) has been operational at Kilpisjärvi, Finland, since September 1994. One of the main purposes of this installation is joint studies with the EISCAT incoherent scatter radar system, whose transmitters are 83 km from the riometer site. We discuss the scope for investigations using combined EISCAT and IRIS data and illustrate some of these with examples. Emphasis is placed on aspects of the ionospheric D-region and mesosphere, but potential areas of exploitation extend to the E-region, the F-region and the magnetosphere, and include ionospheric modification experiments.

The application of IRIS data to help differentiate between spatial and temporal variations in EISCAT measurements is a fundamental strength of such joint studies. In one example of a substorm onset during daylight conditions, the spatial distribution and dynamics of the radio absorption showed a morphology similar to that of visible aurora at substorm onset, including spectral hardening. The IRIS data allowed the dual-beam EISCAT observations to be set in a proper spatial context with respect to the dynamical changes in particle precipitation. A comparison of electric field measurements from EISCAT with the horizontal motions of different types of absorption event revealed no consistent relationship between the two.

1. INTRODUCTION

Riometers have been utilised in many studies of auroral disturbances since the introduction of the technique almost 40 years ago (e.g. Hargreaves, 1969). The measured absorption of cosmic radio noise can be related in general terms to energetic particle precipitation into the lower ionosphere (Collis *et al.*, 1984). Advantages of the method include continuous operation with little upkeep, together with relatively inexpensive installation costs, allowing networks of instruments to be set up.

A limiting feature in standard riometer applications is that the measured absorption represents an integrated ionospheric quantity, defined by the antenna beam-pattern in the horizontal plane, as well as along the beam direction. Typical beam widths are of the order of 60°. Better definition in the horizontal direction has been achieved with the introduction of systems with narrower beams, in particular when these are formed into multiple beams (Nielsen and Axford, 1977; Nielsen, 1980; Kikuchi *et al.*, 1988).

A further refinement of the cosmic-noise technique is the imaging riometer for ionospheric studies, IRIS (Detrick and Rosenberg, 1990). This instrument measures the two-dimensional distribution of absorption with multiple narrow beams (~13° beam width) over an ionospheric area of about 200 km square. The time resolution is 1 s, allowing the spatial and temporal development of absorption regions to be mapped in considerable detail. No height information can be retrieved from these observations, however. Incoherent scatter radar measurements, on the other hand, are especially valuable because of their inherent capacity to provide altitude profiles of ionospheric quantities. In this paper we review the strengths of applying the two techniques together. We present results from the IRIS at Kilpisjärvi, Finland (Hargreaves *et al.*, 1997), and from the EISCAT incoherent scatter radar system in northern Scandinavia (Folkestad *et al.*, 1983; Rishbeth and van Eyken, 1993).

The facilities are introduced briefly with a description of the available data. We then outline the main areas of likely studies, which fall into different categories according to the principle quantities that are derived from the radar observations. The fundamental one of these is D-region electron density, including its inversion to the flux-energy spectrum of precipitating electrons. Incoherent scatter spectral widths have great potential for contributing to studies of D-region

*On leave from EISCAT, Box 812, Kiruna, Sweden.

aeronomy, though their interpretation depends on the availability of ion-chemical models. A specific application in this field is the study of polar cap absorption events, by virtue of their slow variations and high signal-to-noise ratios. For mesospheric studies in general, the Doppler shifts of D-region spectra yield neutral winds, which are likely to be affected by particle precipitation. The dynamics of absorption events can be compared with electric field measurements from the radar. Also, cosmic radio noise may sometimes be absorbed in the E- or F-region of the ionosphere; the radar can be used to investigate these conditions, or indeed to monitor the ionosphere as a whole during precipitation events. Finally, we suggest areas for future studies based on the first year of IRIS observations from Kilpisjärvi and our initial comparisons with EISCAT data.

2. INSTRUMENTATION

2.1. *EISCAT*

The EISCAT radar transmitters are located near Tromsø, Norway, a distance of 83 km from Kilpisjärvi and within the IRIS field-of-view (Fig. 1). The facility consists of a UHF system operating in the 930 MHz band, featuring tristatic reception and fully steerable antennas, and a monostatic VHF system (224 MHz) capable of motion in the north–south plane. Simultaneous operation of the two radars together is now routine. As well as the usual altitude-profile measurements, the tristatic design of the UHF radar allows the determination of vector ion velocities (and hence electric fields). The VHF radar can be configured as a dual-beam instrument with additional, pre-selected pointing in the zonal direction. The time allocated for radar observations is divided equally between common programmes and special programmes, which we now briefly describe.

2.1.1. *Common programmes.* Common programmes (CP) are a set of experiments (presently six) which are run to provide a data base of systematic observations at regular intervals. Durations are typically 1–3 days, though occasional longer runs are also undertaken for particular campaigns. A range of pulse schemes and antenna pointing directions is employed, resulting in some of the CP designs being more useful than others for comparison with IRIS. CPs represent 50% of EISCAT's operations and amount to ~750 h per year. Results from CP operations are available to all the EISCAT Associates.

The experiments are named sequentially from CP-1 to CP-7, where CP-1, CP-2 and CP-3 are run on the UHF system, and CP-4, CP-6 and CP-7 use the VHF. (CP-5 has been discontinued.) All of these schemes include D-region power measurements, from which the electron density can be derived. However, CP-1

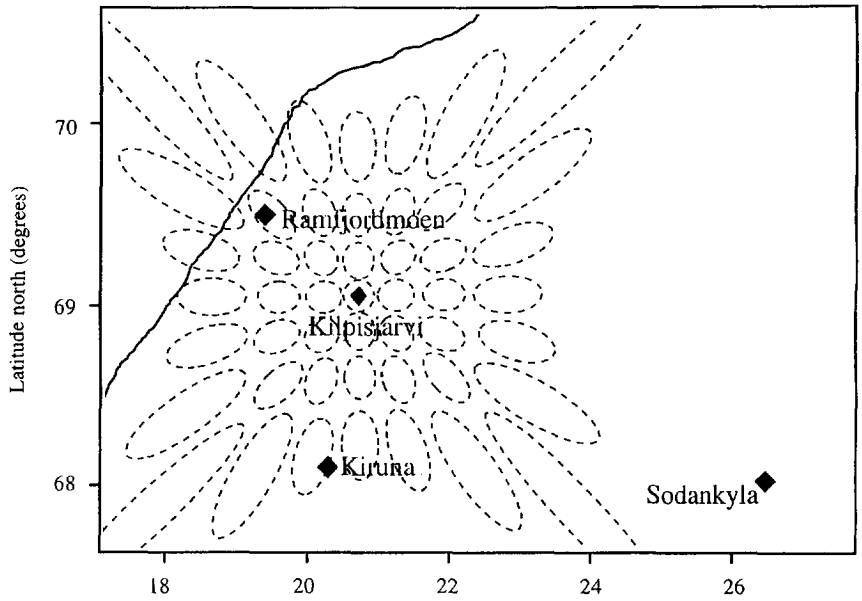

Fig. 1. Outline map of northern Scandinavia showing the locations of the EISCAT sites and the beam pattern (projected to 90 km altitude) of the imaging riometer located at Kilpisjärvi.

and CP-6 are likely to be of most value for IRIS studies by virtue of their fixed pointing and relatively good height resolution. In fact, CP-6 is designed especially for D-region work and is the only one of the above to measure mesospheric incoherent scatter spectra (Turunen, 1986).

2.1.2. *Special programmes.* Special Programmes (SP) account for the remaining 50% of EISCAT's operations. These constitute experiments run for specific purposes by individual scientists of the EISCAT Associates. The available time is divided amongst the Associates in a pre-determined way. Thus it is possible to design an experiment especially to provide the information most relevant to IRIS studies, and to run it when desired. While valuable data can certainly be obtained in this way, the observing time is limited and the majority of interesting events will occur during CP operations.

2.2. *The imaging riometer at Kilpisjärvi*

The Kilpisjärvi IRIS consists of a 64-element dipole array, phased to form 49 individual beams as shown in Fig. 1. Half-power beam-widths near the zenith are of the order of 20 km horizontally in the D-region. One of the beams intersects the ionosphere at 90 km altitude directly above the radar site. This is particularly suitable for comparisons with radar experiments using vertical pointing (a common choice for the VHF system). The IRIS operating frequency is 38.2 MHz and observations began in September 1994. Raw data are recorded at 1 s resolution, though averaging is often used for subsequent analysis (Hargreaves *et al.*, 1996).

A full technical description of the system is given by Detrick and Rosenberg (1990). Minor modifications to the Kilpisjärvi IRIS include the riometer design, a timing system based on GPS and the inclusion of lightning protection. Standard broad-beam riometer measurements at the same frequency are also available.

3. IONOSPHERIC PARAMETERS DERIVED FROM INCOHERENT SCATTER RADAR MEASUREMENTS

The standard quantities measured by the incoherent scatter radar technique are the electron density, the temperatures of the ions and of the electrons, and the ion velocity. From the latter, the ionospheric electric field can be determined, along with the neutral wind in the D- and E-region. In the lower ionosphere, where the collisions of ions with the neutral atmosphere affect the shape of the backscattered spectrum, the ion-neutral collision frequency can be estimated. The change in average ion mass, from NO^+ to O^+ in the E/F transition region, may also be studied. Beyond these basic quantities, a range of parameters describing the ionised and neutral atmosphere may be investigated (e.g. Evans, 1969), though these are beyond the scope of the present article.

In comparisons with IRIS measurements, radar observations of the ionospheric D-region are of particular interest. The principal quantity is the electron density as a function of height and time. Resolutions of the order of one or two kilometres, and no more than a few seconds, are required to accurately monitor the main features of D-region conditions during dynamic events. Another quantity of importance in such studies is the measurement of the backscatter spectrum from mesospheric heights. This contains information on mesospheric neutral winds (from the Doppler shift) and on aeronomy (from the spectral width). We address the various areas of interest below and illustrate their potential with the use of observations from the initial period of IRIS operations. This overview of combined EISCAT/IRIS studies does not allow the various events reported here to be studied in depth. We expect to develop individual studies for publication elsewhere.

3.1. *D-region electron density*

As the radio wave absorption measured by IRIS is almost exclusively the result of increased electron density in the D-region (see Section 3.7 for other causes), this quantity is fundamental to joint IRIS and radar studies. It is also the easiest parameter to derive from the radar measurements. In most cases the density is simply related to the backscattered power; exceptions include phenomena when incoherent scatter is not the sole scattering mechanism, such as polar mesosphere summer echoes (Collis and Röttger, 1990). We consider here an example in which both radars were operating simultaneously and pointing in different directions. This arrangement allows the two-dimensional map of absorption from IRIS to be compared with two spatially-separated profiles of D-region electron density within that map.

During the experiment in question, on 4 May, 1995 the VHF radar was pointing vertically, providing power and spectral measurements at 1.05 km increments between 70 and 112 km altitude with 10 s resolution. The UHF radar was pointed to intersect the D-region at 90 km altitude vertically above Kilpisjärvi, requiring an elevation of 46.8° towards the south-east (Fig. 2). Power measurements were obtained every 3.15 km in range, starting at 63.7 km range. This translates to every 2.3 km in altitude,

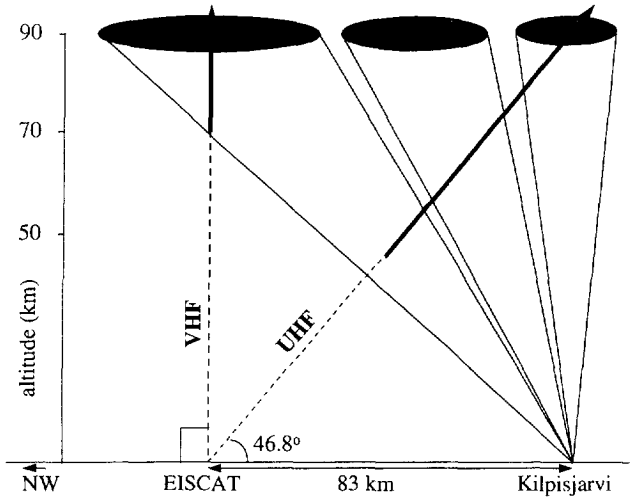

Fig. 2. Sketch of the geometry of the EISCAT experiment used on 4 May, 1995. The lines labelled UHF and VHF refer to the pointing directions of the two radar beams; the full-line sections indicate the ranges from which measurements were taken (both extend beyond 90 km altitude). Also shown are three of the IRIS beams which lie in the NW–SE plane.

starting at 46.4 km altitude with the adopted antenna pointing. Raw data were recorded every 5 s.

Figure 3 shows the electron density measured by the VHF radar at four selected heights between 82.6 and 92.1 km over a 30 min interval. A sudden increase occurred at 1824:30 UT, with no significant preceding activity. Two minutes after the onset, the densities below 85 km were dramatically, but briefly, enhanced, relative to those above 90 km, indicating a region of more energetic precipitation following the main onset by a couple of minutes. The geomagnetic signature of this event, as measured by the X-component at Kiruna, was an impulsive increase of 150 nT, followed by a subsequent reduction by 500 nT over the following 20 min; at Tromsø the D-component made a transient excursion of 1.3° (data not shown here).

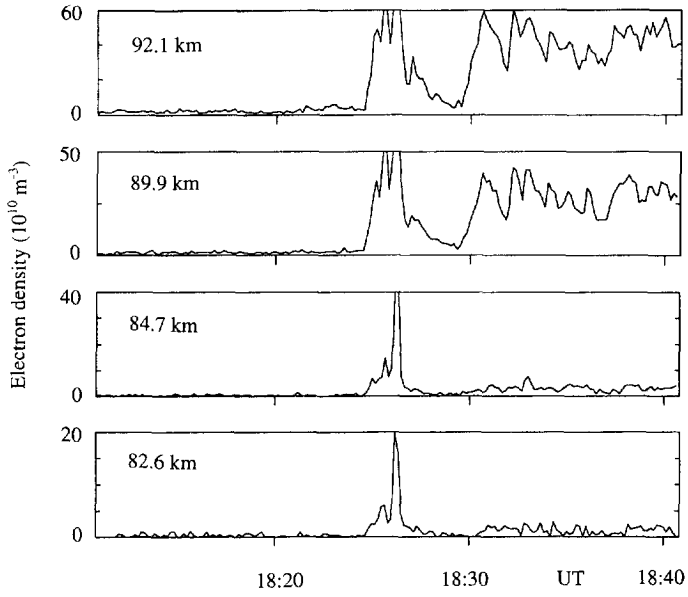

Fig. 3. Time series of EISCAT VHF data from the 4 May sharp onset event. Each plot covers 30 min and shows the electron density at heights of (top to bottom) 92.1 km, 89.9 km, 84.7 km and 82.6 km. The antenna was pointing vertically.

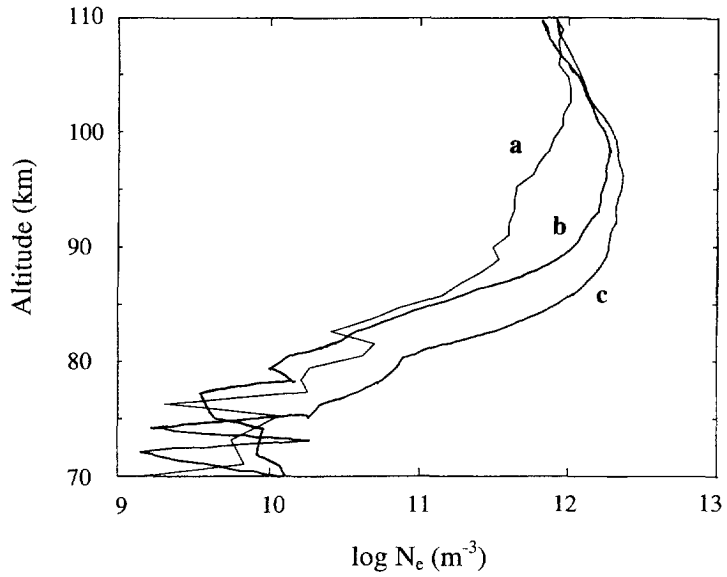

Fig. 4. EISCAT VHF electron density profiles from 4 May onset. Each profile is a 10 s average starting at (a) 1825:40 UT, (b) 1825:50 UT and (c) 1826:00 UT.

Three consecutive electron density profiles (10 s resolution) observed by the VHF radar at this time are displayed in Fig. 4. The maximum values are very large, of the order of $10^{12}\,m^{-3}$ near the peak at 95 km. It is possible that the densities may be overestimated if the calibration of the radar (or the data analysis) was in error. However, in a study of absorption spike events using the Chatanika incoherent scatter radar, Hargreaves (1980) found the electron density to typically exceed $10^{12}\,m^{-3}$ at 90 km altitude for short intervals (15 s averages). Also, brief enhancements in excess of $4\times10^{12}\,m^{-3}$ at 105 km have been reported on the basis of EISCAT measurements (Lanchester *et al.*, 1994). EISCAT observations during another event found almost $4\times10^{12}\,m^{-3}$ at 98 km (Aikio and Kaila, 1996), so we tend to believe the values in Fig. 4. The inversion of the EISCAT VHF profiles in Fig. 4 to electron energy spectra is described in Section 3.3.

Figure 5 indicates that the UHF radar, looking 80 km distant, detected an onset at exactly the same time as the VHF radar, but it is difficult to match individual density variations in the two beams thereafter. A further significant feature to note in Fig. 5 is that the electron density at 90 km altitude and above showed a brief enhancement about 10 min before the onset over Kilpisjärvi. Observed alone, the two sets of measurements in Figs 3 and 5 could lead to different interpretations of conditions at substorm onset. It is only when we also include the information from IRIS that the spatial relationships of these observations can be put in context.

We introduce some of the IRIS data from this event in Fig. 6. These serve to illustrate the overall quality, as well as the spatial and temporal detail available from the observations. Individual IRIS beams are identified by a pair of numbers (row, column), where rows are E-W and columns N-S (Fig. 1), relative to the zenith beam (0,0) above Kilpisjärvi (with north and east counted positive). The two panels in Fig. 6 show a N–S (left) and E–W (right) selection of beams, each passing overhead of the radar location (with that IRIS beam, (2, −2), being common to both panels). The horizontal distance spanned by each set of four beams (between the centres of the outside beams at 90 km altitude) is about 100 km. However, the upper beams in each panel are at the northern (3, −2) and western (2, −3) edges of the array, and include significantly more spatial integration than the inner beams (see Fig. 1). This is probably why the outer beams showed less structure than the others at the onset (Fig. 6). Note that to the east of EISCAT there were three absorption maxima within the onset, while in the beam to the south there were only two and in the next one further south there was only one clear maximum. Thus there were distinct differences in the nature of the precipitation over spatial scales of the order of 50 km at the onset.

The temporal and spatial development of the radio absorption observed by IRIS over the period covered by the EISCAT data in Figs 3 and 5 is displayed in Fig. 7. A latitudinally-confined feature spread rapidly across the IRIS field-of-view between 1813 and 1815

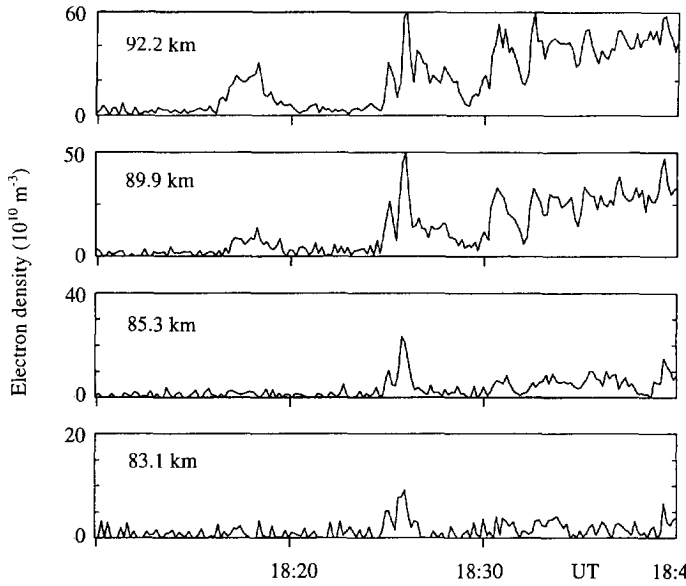

Fig. 5. As Fig. 3 but for the EISCAT UHF radar. The altitudes are approximately the same as in Fig. 3 but differ slightly because of the geometry. From top to bottom they are: 92.2 km, 89.9 km, 85.3 km and 83.1 km. The antenna was pointing at an elevation of 46.8° and azimuth 135°.

UT, with its poleward edge close to Kilpisjärvi. This is the relatively soft precipitation seen at that time by the UHF radar pointing over Kilpisjärvi. The elongated form then moved equatorwards over the next few minutes, out of the UHF radar beam and without ever having reached the vertically-pointing VHF beam. At 1822 UT the absorption briefly decreased (Fig. 7, image 6 in the third row down). This was just before the sharp onset entered the IRIS area from the east at 1824 UT. The leading edge of the onset reached the western boundary of the IRIS field-of-view in less than 2 min (Fig. 7, images 1–4 in the fourth row down).

The IRIS images in the period up to, and including, the onset are graphically similar to some observations of visible aurora near substorm onset. In a study using a network of broad-beam riometers and all-sky camera data, Collis and Korth (1983) reported a delay of about 2 min between the passage of a visible westward travelling surge and a sharp onset of radio absorption. Equatorward motion, temporary fading and westward expansion of the precipitation region are all well-documented from optical observations (e.g. Kauristie *et al.*, 1995). We thus conclude that, at least in this case, the substorm morphology of ~few keV electrons manifested in optical observations also applies for the electrons of higher energies (~few tens keV) that produce radio absorption. However, as this event occurred during the polar summer, we are not able to compare the observations with optical data, though we do plan to do this with suitable events in the future.

The above example illustrates the well-known difficulty of interpreting monostatic radar data in terms of spatial or temporal variations. Dual-beam radar observations provide more information, but the spatial context of the energetic precipitation can only be provided by an imaging riometer.

3.2. *Energy spectra of precipitating electrons*

The electron density in the D-region represents the balance between the ionisation rate caused by incoming charged particles and the recombination rate of the ionospheric ion species. Using models for the neutral atmosphere and a profile of effective recombination coefficients, together with a model for the energy deposition as a function of atmospheric depth, it is possible to determine the energy spectra of the incoming particles from the observed electron density profile. Details of the application of this method have been given by Hargreaves and Devlin (1990).

The density profiles shown in Fig. 4 have been inverted to particle fluxes to illustrate how the energy spectrum changed through this onset (Fig. 8). The overall hardening of the spectrum during this 30 s interval is clear. However, it should be noted that the absolute flux values and the detailed shapes of the spectra depend on the assumed atmospheric model,

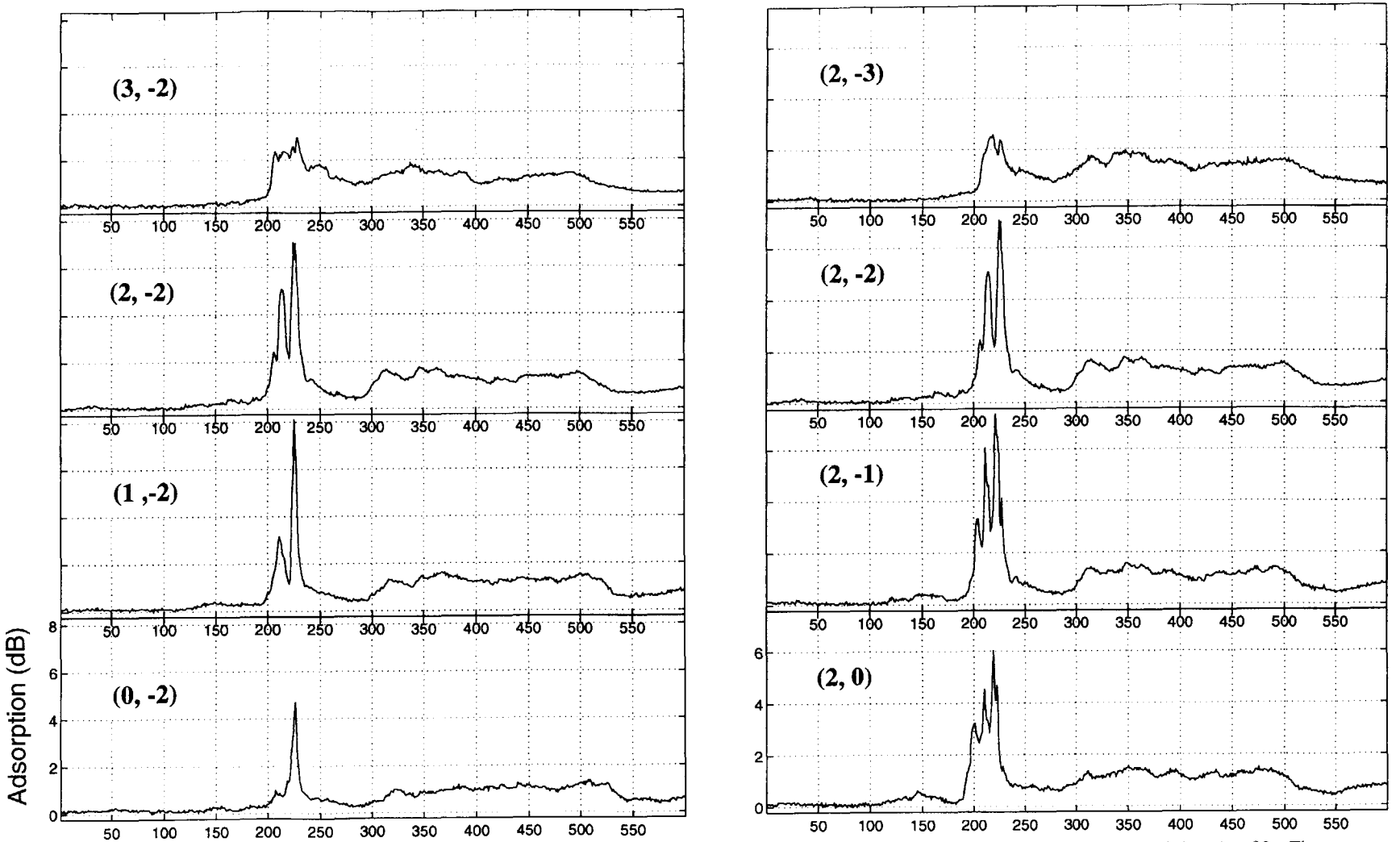

Fig. 6. Radio absorption measured by individual IRIS beams between 1815 and 1845 UT on 4 May, 1995. The data are 3 s averages and the time scale is in units of 3 s. The left panel shows four adjacent beams from the N–S column passing overhead of EISCAT, and the right panel similarly for an E–W row. The left panel runs (top to bottom) from the northern edge of the array to the centre row, and the right panel from the western edge to the centre column (see Fig. 1). The beam numbering convention is described in the text.

particularly the effective recombination coefficients.

As well as the inferred electron flux, the algorithm also provides height profiles of ionisation rate and incremental absorption. Thus, as a self-consistency check, the total calculated radio-wave absorption can be compared with that actually observed. For the case presented here, the maximum instantaneous absorption recorded by the riometer beam pointing directly over EISCAT was 7 dB, at 1826:10 UT. The absorption predicted from the profile for this time was 6.2 dB, which may be considered excellent agreement with the observation.

The empirical approach described above has the advantage of depending mainly on simple ionospheric parameters. These may readily be adjusted for particular case studies, allowing an easy insight into the physical processes. Moreover, the calculations are not especially computer-intensive. A more advanced method, examining the details of the ion chemistry underlying the bulk parameters, considers individual ionic reaction rates (Burns *et al.*, 1991). Yet more refined, and an area of considerable promise, is a technique that uses spectral width measurements, as well as electron density, from the radar (Turunen, 1993). We consider spectral widths in Section 3.4.

3.3. *Electric fields*

The magnetospheric electric field is a key element in understanding the dynamics of auroral events. The electric field maps down to the ionosphere, where the induced ion drifts can be measured by incoherent scatter radar. Tristatic reception of scattered signals from the EISCAT UHF radar allows the simultaneous measurement of three line-of-sight ion velocity components. These can then be combined to determine the full vector ion drift, and hence the electric field.

The collocation of EISCAT and the Kilpisjärvi IRIS offers a unique opportunity to compare high-resolution ground-based electric field observations with the motions of absorption events. We present results here from two different types of event: a daytime event drifting very slowly equatorwards, and a night-time event moving rapidly polewards.

3.3.1. *Slowly drifting daytime event.* Figure 9 displays the radio absorption observed by the Kilpisjärvi IRIS just after local noon on 1 March, 1995. This event was unusual in two respects. First, it was relatively localised and kept its form for about 2 h while drifting very slowly westwards and equatorwards. Despite this slow drift motion, if we consider the rotation of the earth it is immediately apparent that the precipitation region is in fact almost exactly co-rotating with the earth. (A fixed position in the magnetosphere–ionosphere system, with respect to the sun, crosses the 200 km width of the IRIS field-of-view in about 20 min.) Without presenting the data here, we note that a second characteristic was that the electron precipitation during this event was hard, with a peak in electron density below 90 km altitude (corresponding to electron energies of ~ 50 keV). Increases in electron density were observed down to 65 km, the lowest height covered by the EISCAT experiment, implying the presence of some electrons with energies 500 keV or greater. This event is discussed in more detail by Collis *et al.* (1996); here, we will deal only with the drift motion of the absorption feature and the EISCAT F-region ion drift velocities.

In this experiment, the radar provided continuous observations of ion drifts at an altitude of 278 km on the field line passing through the transmitter site. These measurements are thus very localised, and in using them in comparison with the motion of absorption features from IRIS we are assuming that there is little change in electric field over horizontal distances of up to ~ 100 km or so. This seems to be a good assumption in the present case as the drifts varied slowly and rather uniformly with time. The drifts from IRIS were well defined between about 1130 and 1230 UT, and less well-defined, though with small-to-zero trends, after this time. These two phases correspond to when the event was relatively strong (1.5 to 2.5 dB), and diminishing (below 1 dB), respectively. The event was in the radar beam between about 1155 and 1230 UT.

At 1100 UT, some 30 min before the absorption event entered the IRIS viewing area from the north-east, the EISCAT F-region ion drifts were mainly westward (400 ms^{-1}) with a small (100 ms^{-1}) poleward component (Fig. 10). The 'noise' level in these values is $\sim \pm 50$ ms^{-1}, which may constitute actual geophysical variations as well as stochastic measurement noise. Both components then decreased gradually to approximately zero over the next hour. The components of motion of the absorption feature are also shown in Fig. 10, indicating that the drifts observed by the two techniques were both quite small during this interval, tending to zero when the absorption event was crossing the radar beam. Note that we are not advocating a causal relationship between the F-region convection and any motion in the mesosphere. Rather, the drift of the absorption patch is almost certainly that of a source region in the magnetosphere. Before the absorption event reached the radar beam it could be identified clearly as moving westwards and equatorwards. The westward motion during this initial phase matched the EISCAT ion drift well, but the small equatorward component was approximately

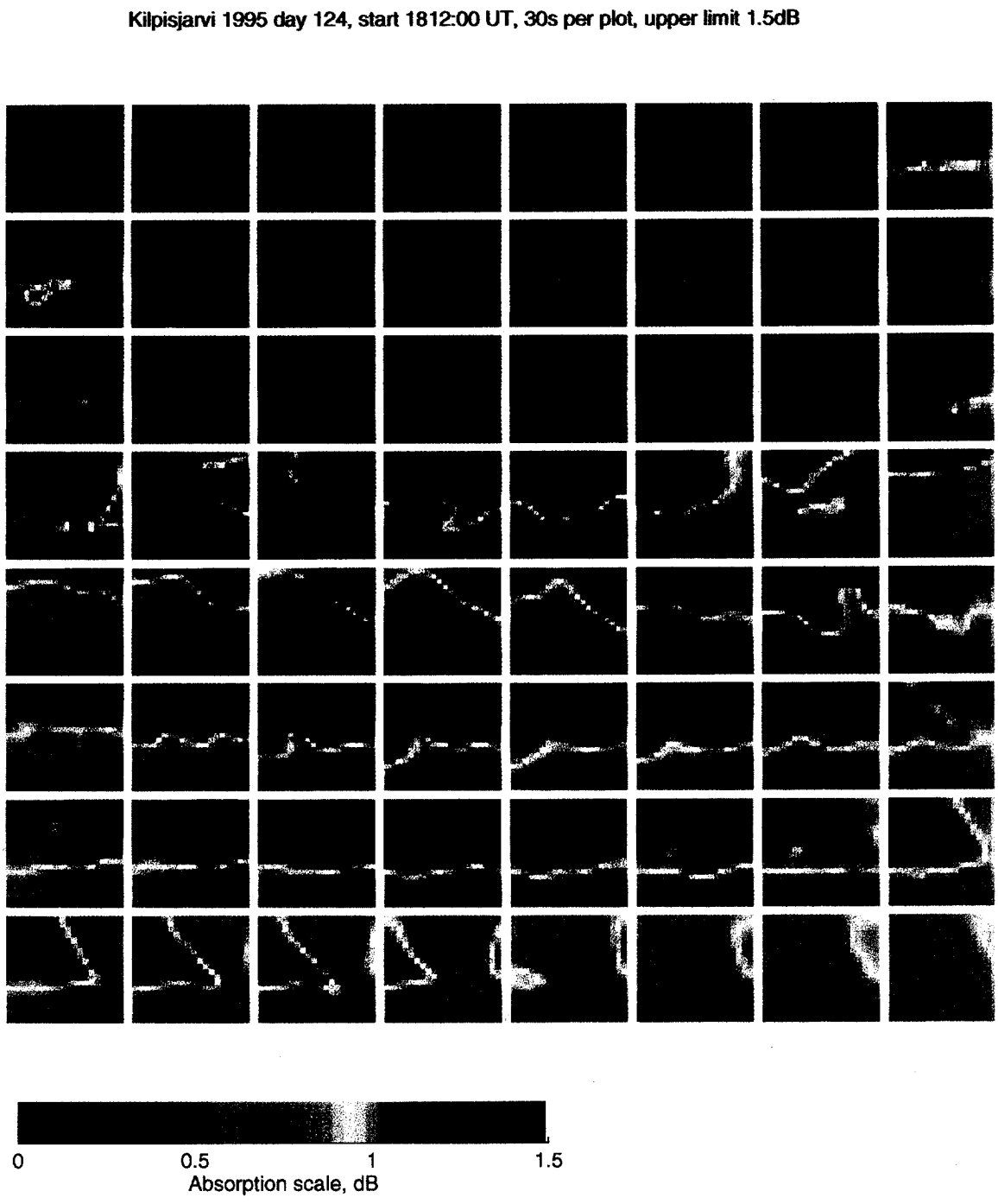

Fig. 7. Horizontal distribution of radio absorption derived from the Kilpisjärvi IRIS observations on 4 May, 1995. Each plot extends over 240 km in both the N–S (vertical) and E–W (horizontal) directions by projecting each IRIS beam to 90 km altitude, looking down on the ionosphere. The top left image corresponds to 1812 UT; successive 30 s intervals run from left to right along each row, progressively from top to bottom. The colour scale is saturated at 1.5 dB to highlight the weaker E–W elongated feature preceding the sharp onset at ~1824 UT which reached peak values of 7 dB. EISCAT's location is midway between the centre and the top left corner of each image.

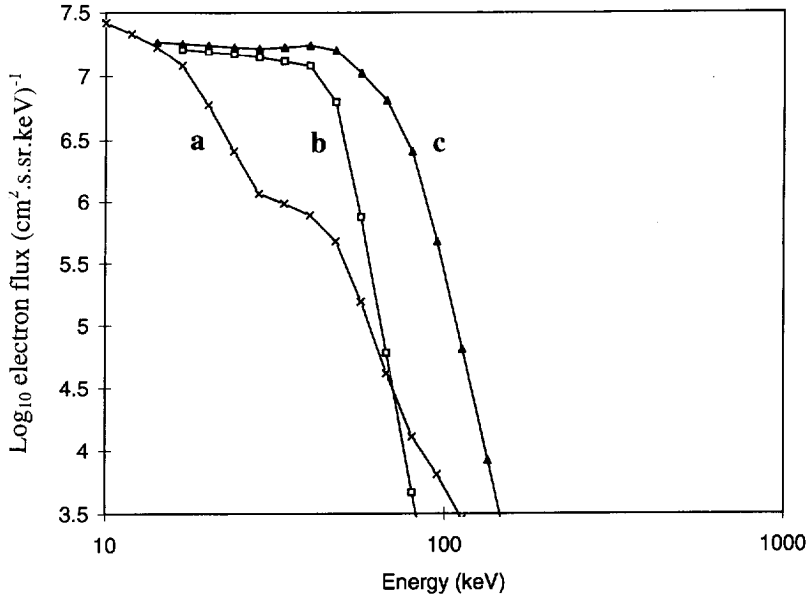

Fig. 8. Inferred flux-energy spectra corresponding to the electron density profiles shown in Fig. 4. Each profile is a 10 s average starting at (a) 1825:40 UT, (b) 1825:50 UT and (c) 1826:00 UT.

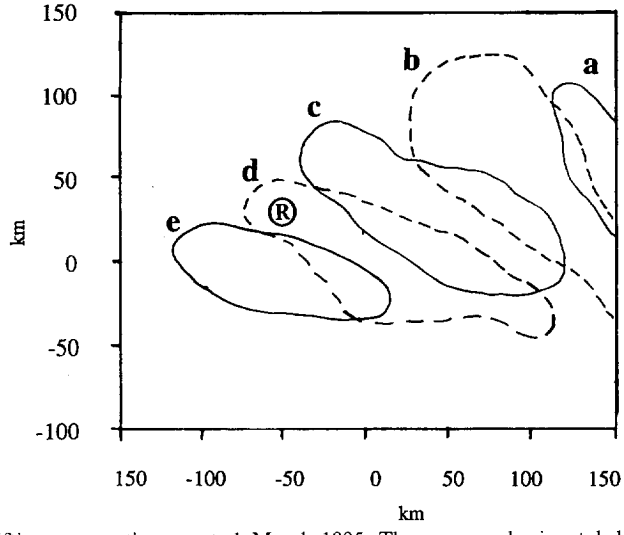

Fig. 9. Slowly drifting, co-rotating event, 1 March 1995. The axes are horizontal distance centred on Kilpisjärvi (0,0), positive north and east, assuming a height of 90 km for the absorption. The contours show the position of the event, defined by the 1 dB boundary, at the following times: (a) 1134 UT, (b) 1146 UT, (c) 1154 UT, (d) 1210 UT and (e) 1250 UT. The location of the radar beam in the D-region is marked ®.

opposite to the poleward convection seen by the radar. This may mean that the meridional E-field component causing the westward drift was fairly uniform for 100 km or so to the north-east of the radar, but that the zonal E-field component probably changed sign.

3.3.2. *Rapid poleward expansion.* A recurring feature in the IRIS data set is a latitudinally-confined absorption region propagating polewards at high speed. These tend to occur at event onsets and, as viewed with a single riometer beam, have a sudden beginning, a short duration and often high intensity, i.e. a spike-like character (Hargreaves *et al.*, 1997).

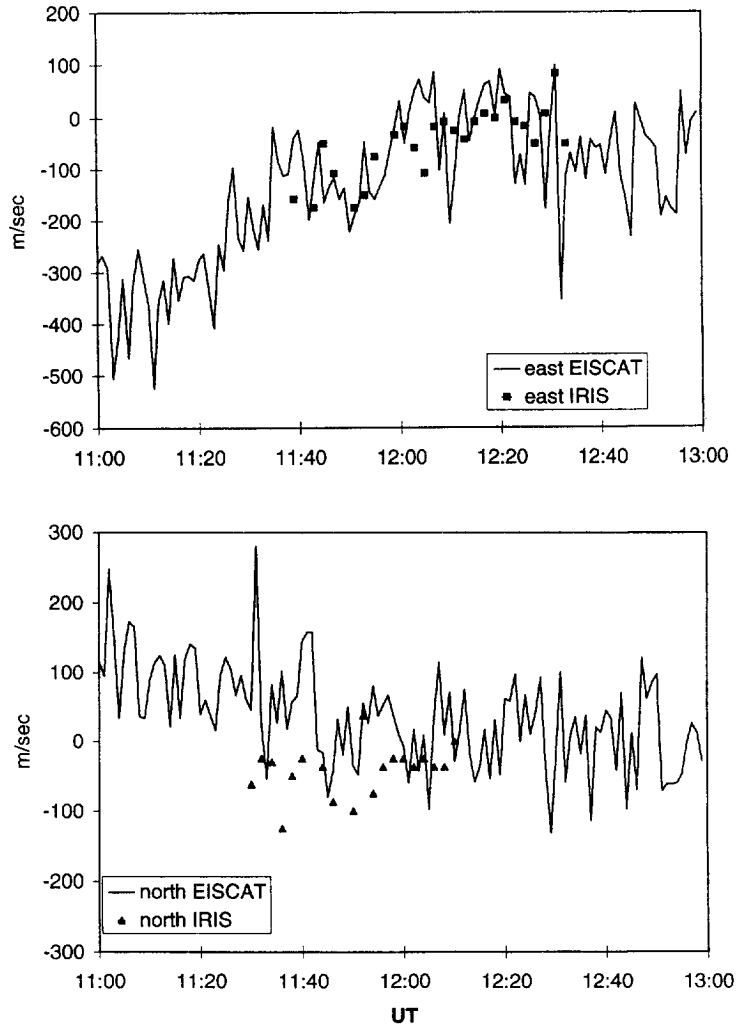

Fig. 10. EISCAT and IRIS drifts for the 1 March event shown in Fig. 9. The full lines are 1 min averages of the horizontal F-region velocities from EISCAT, positive east (top) and north (bottom). The symbols show the respective drifts of the absorption event, determines from the location of the maximum absorption every 2 min.

One such event occurred on the evening of 28 February, 1995 passing the EISCAT location just after 1933 UT (Fig. 11). This feature crossed from the south-east to the north-west corners of the IRIS field-of-view in 200 s, suggesting components of motion of 1 km s^{-1} both polewards and westwards. The structure was elongated in the ENE–WSW direction, or approximately parallel to the local L-shells and extended beyond the IRIS field-of-view. With this alignment, the actual motion of the feature could be either entirely polewards, or entirely westwards, or indeed anywhere between, while the second component arises as an artefact of the orientation. The actual motion is not important for the present purposes; it is sufficient to know that the direction was somewhere between northwards and westwards, and the speed was of the order of 1 km s^{-1}.

The rapid motion of this event means that we need to examine the EISCAT data with high time resolution. This necessarily introduces increased statistical uncertainties into the estimates. As a compromise between reducing excessive noise and still resolving the event, we show in Fig. 12 the horizontal ion drifts using 10 s averages (the raw data have 5 s resolution). There are large point-to-point differences in both sets of results, though in the period 1932–1935 UT when the absorption feature traversed the region they tend to have consistent values of up to about 1 km s^{-1}. The

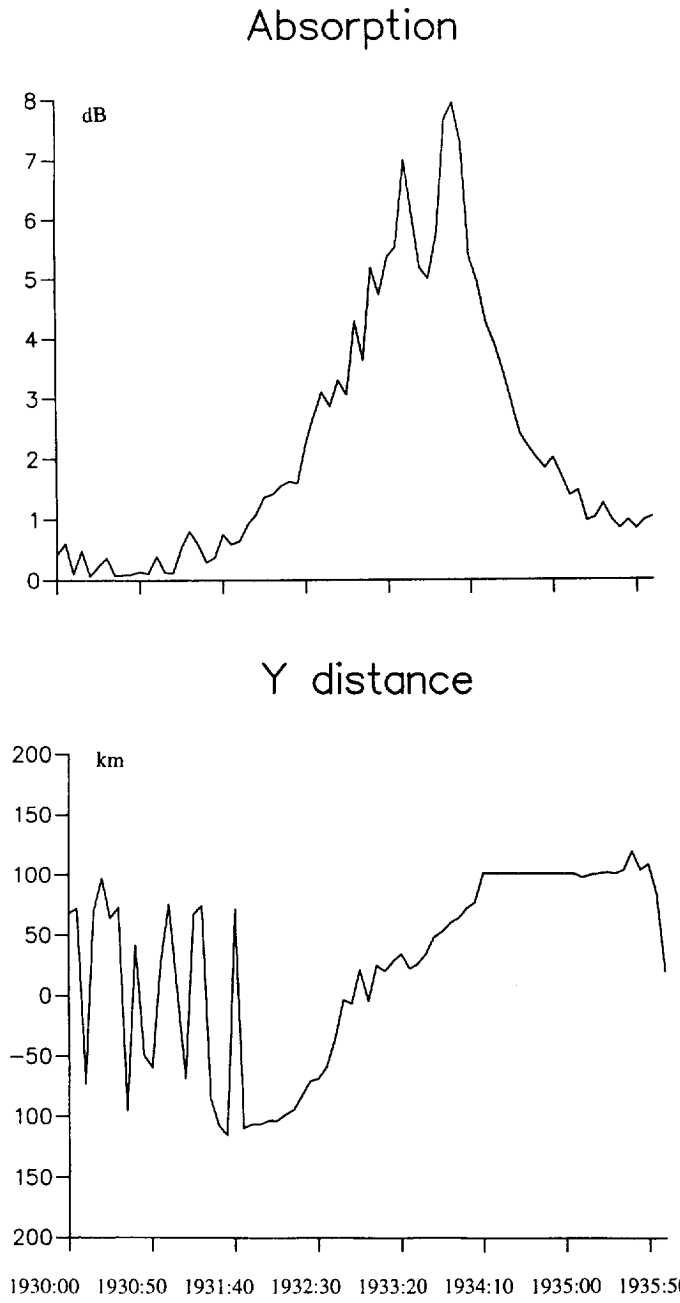

Fig. 11. Poleward-propagating absorption event on 28 February, 1995. The top panel shows the maximum absorption recorded by IRIS, irrespective of which of the 49 beams it was detected in. The lower panel shows the N–S location (Y distance) of the peak with respect to Kilpisjärvi (positive north). Variations in Y prior to 1931:40 UT are noisy because no clear maximum existed. The flat section after 1934:10 UT indicates that the peak was beyond the poleward edge of the field-of-view. The poleward motion between 1932 UT and 1934 UT has a mean value of 1.3 km s^{-1}.

zonal component was westwards, and switched sign momentarily just as the precipitation reached the radar. This could be the same phenomenon of an enhanced perpendicular electric field observed in relation to visible auroral forms (Opgenoorth *et al.*, 1990), but in this case the auroral form is also

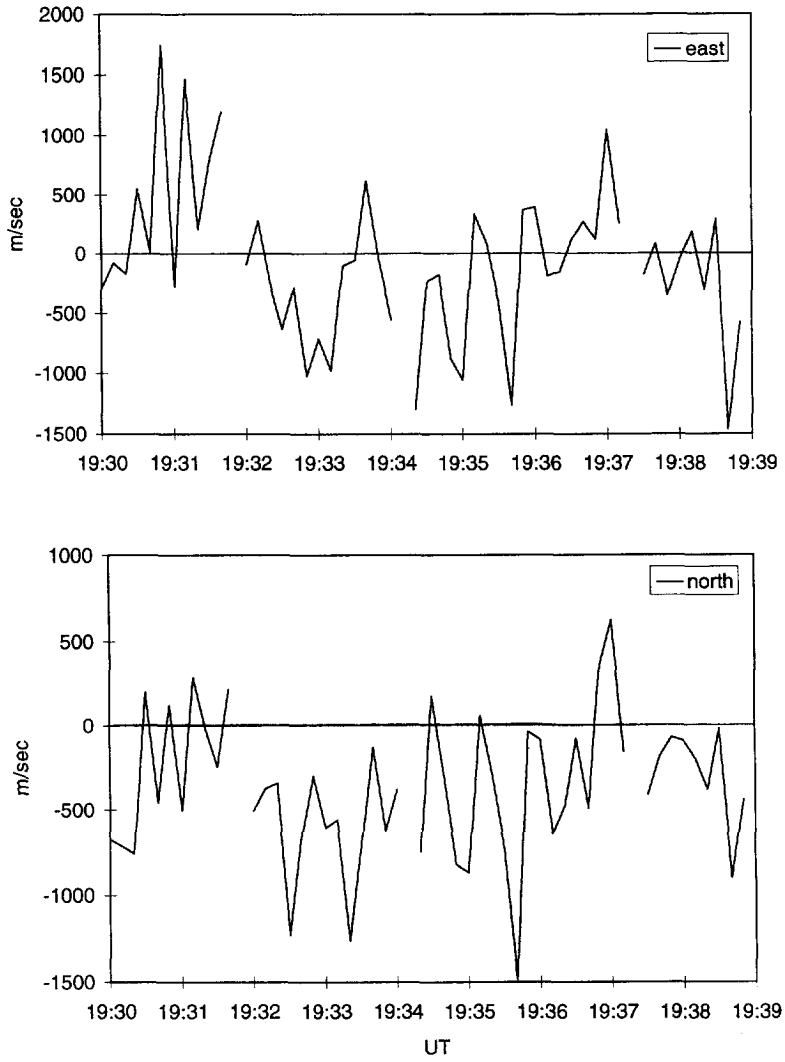

Fig. 12. EISCAT F-region drifts (10 s averages) during the interval on 28 February shown in Fig. 11. The zonal component (positive east) is shown in the top panel and the meridional (positive north) in the lower panel.

sufficiently energetic to be an absorption event. The meridional component is, however, equatorwards, and so is opposite to the motion of the absorption event. It is clear that many more events will need to be studied to reveal whether any relationship exists between the motions of absorption events and of ion drift in the ionosphere.

3.4. *Spectral widths*

The incoherent scatter ion line measured at mesospheric heights is severely damped by ion-neutral collisions, producing a very narrow, single-peaked spectrum, which turns out to be of Lorentzian shape (Mathews, 1986). This leads to relatively simple analytical fitting routines, describing the spectral shape by its amplitude, width, base level and Doppler shift (Rietveld and Collis, 1993). The observed Doppler shifts allow wind measurements as described in Section 3.6. The spectral width (defined as the full-width at half-maximum amplitude) depends on the complex aeronomical processes at the height of the measurement. Thus, in principle, it is possible to predict the widths with good enough aeronomical models. In practice, some assumptions, or supplementary observations from other sources, are used to limit the degrees of freedom in parameter fitting.

In broad terms, the spectral width depends on the ratio N/T of number density (N) to temperature (T) of the neutral atmosphere, and on the number densities and masses of both positive and negative ion species (Rietveld and Collis, 1993). The significance of the IRIS data lies in the expected dependence of all of these quantities on the ionisation rate. While the electron density measurements from the radar show when precipitation is in progress within the radar beam (from which the ionisation rate may be deduced as in Section 3.2.), the spectral widths can be influenced by thermal and chemical processes originating elsewhere. Thus the spatial distribution of precipitation from IRIS is important.

The spectral width is affected profoundly by changes in the ratio of negative ion number density to electron number density, a quantity usually termed λ. The width is essentially proportional to $(1+\lambda)$, and clear changes have been observed during polar cap absorption (PCA) events through twilight when the number density of negative ions undergoes change (Rietveld and Collis, 1993; Turunen, 1993). The special case of PCA events is discussed in the following section.

There have been several studies of spectral widths *per se* in the literature, but changes of this quantity during electron precipitation events have not been reported in detail. One expectation is that the transition height from mainly molecular ions to mainly cluster ions in the 80–90 km altitude region ought to be observable. This height is expected to be reduced as the production rate increases. However, since the radar requires a significant ion production rate before spectra can be resolved (because of signal-to-noise ratio considerations), the scope for such investigations depends on which of the ion chemistry or the radar is the more sensitive to changes in the production rate.

To illustrate the potential of such studies, we consider the spectral widths measured during the 2 h period including the substorm onset on 4 May 1995, discussed earlier. Figure 13 illustrates the electron density and spectral width from 90 km altitude. Note that these are averages over 150 s to allow better estimates of spectral width during periods when the electron density was low; the maximum density at the onset is thus smaller than the instantaneous (10 s) values shown in Fig. 4. The spectral width estimations prior to the sharp increase of electron density at ~1825 UT are unreliable because of low signal levels, so it is difficult to assign a value for the undisturbed ionosphere. However, following the onset, the spectral widths decreased dramatically from ~75 Hz to ~50 Hz over an interval of 40 min, then increased again to ~65 Hz over the next 30 min. A decrease in spectral width can result from a decrease in negative ion number density, a decrease in N/T or an increase in positive ion mass (or some combination of these, of course). In the absence of independent information on one or more of these quantities, we cannot determine unambiguously the cause of the changes. We speculate, however, that the most likely explanation in this case may be atmospheric heating resulting from

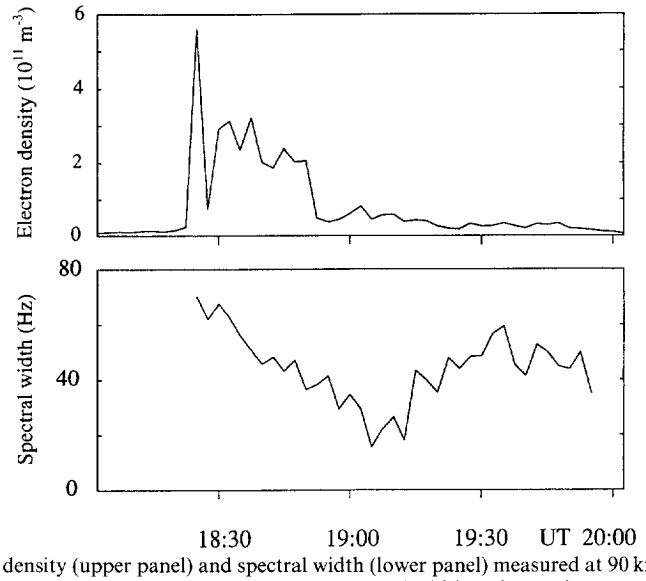

Fig. 13. Electron density (upper panel) and spectral width (lower panel) measured at 90 km altitude during the sharp onset event on the evening of 4 May, 1995. Spectral widths prior to the onset and at the end of the displayed interval were not fitted reliably because of low signal-to-noise ratio.

the intense precipitation in the early part of the event, causing an increase in T and a decrease in N (resulting from expansion), with subsequent recovery as the precipitation decreased in intensity just before 19 UT. The ability to include aeronomical model results in future studies will be of major benefit to the interpretation of the observations.

3.5. *Polar cap absorption events*

The D-region events detected by EISCAT and IRIS are normally caused by the precipitation of electrons into the mesosphere. Protons with energies of several MeV or more can also penetrate to the same heights, or lower. Such events (solar proton events, SPE) are observed preferentially near sunspot maximum, and tend to be long-lived, lasting up to several days. The term polar cap absorption (PCA) is applied to this phenomenon because the protons cause absorption of HF radio waves in the earth's polar regions, over the polar cap and down to some cut-off latitude at about 60° geomagnetic.

The characteristics of such events observed by riometer are often of intense absorption (though weaker events also occur), varying slowly in response to the gradual changes in proton fluxes. The latter are routinely monitored by spacecraft. For a constant proton flux, the observed radio absorption decreases dramatically as the sun sets at mesospheric heights, with a corresponding increase at sunrise. We address this feature below. PCA events are especially useful for mesospheric studies because ionisation is produced at much lower altitudes than during electron precipitation events, providing an incoherent scatter radar target at heights not normally accessible to the technique. Measurements as low as 50 km have been obtained by EISCAT (Collis and Rietveld, 1990).

No PCA event has yet occurred during the operation of IRIS, so we are unable to present a direct comparison of the data here. However, information on the spatial extent and distribution of absorption from IRIS during PCA events is expected to enhance the interpretation of the radar data in studies of at least three phenomena.

First, the twilight changes in absorption, which are understood as being caused by increases in λ at night as free electrons attach to neutral molecules, forming negative ions. The reduction in electron densities and increase in negative ion densities (detected by increases in the spectral width) are clearly observed by radar (Rietveld and Collis, 1993; Turunen, 1993). The rates of change at sunset and sunrise are different, however, probably reflecting different time constants in the chemical changes affecting λ (Collis and Rietveld, 1990). The ability to set the pencil-beam radar observations precisely within the twilight absorption variations mapped by IRIS will be a valuable complement to studies of the ion chemistry.

A second use of the IRIS data is to map the location of the equatorward boundary of the proton precipitation. This is important if the radar data are to be compared with proton flux measurements from spacecraft, since if the radar is on the boundary of the precipitation region it is possible that not all the proton flux observed in space will reach the latitude of the radar.

A third topic, of similar nature to the previous one, is that of the midday recovery, a term applied to a temporary decrease in radio absorption sometimes observed around local noon during a PCA. The cause of this phenomenon is not well known (Hargreaves *et al.*, 1993; Ranta *et al.*, 1995). IRIS should be able to map the spatial and temporal development of this feature, allowing proper interpretation of the radar observations.

3.6. *Winds and waves*

Spectral measurements obtained from mesospheric heights by EISCAT are usually Doppler-shifted. Although the implied motion is that of the ions, it is usual to equate this directly with the line-of-sight component of the neutral wind because the ions move with the neutrals, resulting from the very high ion-neutral collision frequencies at these heights. For experiments with a vertically-pointing antenna, the result is just the vertical wind. For oblique pointing directions, the line-of-sight observation is usually resolved into the horizontal component, as this is normally much larger than the vertical one.

Wave-like phenomena, on a range of time scales, are a common feature of the velocity field measured by the radar. Periods can range from a few minutes to many hours. Waves with periods of 9–14 h and vertical wavelengths of the order of 10 km dominate the velocity field in the height range 50–80 km during PCA events (Rietveld and Collis, 1993). Because the radar cannot observe the middle mesosphere in the absence of precipitation, it is an open question whether the waves are pre-existing, or whether the SPE causes them or modifies them (Röttger, 1994). This line of reasoning also applies to the shorter period waves observed during electron precipitation events. However, as the radar is usually able to make meaningful observations in the upper mesosphere during weak precipitation, or even reasonable solar illumination, changes to the velocity field associated with variations in production rate on a range of time scales

can be examined. This possibility is not available during PCA events as the production rates tend to be much more slowly varying.

Using IRIS data in such studies will permit an overview of the precipitation in the area surrounding the radar beam, rather than having the radar alone as a monitor of precipitation. Thus it may be possible to relate changes in the wind field with activity away from the radar beam.

3.7. *The E-region and F-region during absorption events*

Some weak radio absorption events have been ascribed to processes in both the E-region and the F-region. Stauning (1984) proposed that absorption in the E-region may be expected during periods of E-region electron heating caused by unstable plasma waves, based on observations in conjunction with the Søndre Strømfjord incoherent scatter radar. Such heating events are not uncommon in EISCAT data, though the expected levels of absorption are smaller than the normal D-region events which may also occur during the same disturbance.

A second class of absorption event observed in the absence of energetic particle precipitation has been suggested as being caused by patches of high F-region electron density (Rosenberg *et al.*, 1993; Wang *et al.*, 1994). No observable effect is expected for f_0F2 values less than about 6 MHz, but the predicted absorption increases rapidly for larger critical frequencies, reaching 1 dB (for a 38.2 MHz riometer) at $f_0F2 \sim 12$ MHz.

The above two types of event were observed at very high latitudes, allowing easier distinction from the more usual (and larger) D-region events at auroral latitudes. Nevertheless, EISCAT is an excellent diagnostic tool to investigate whether similar effects may be present in the Kilpisjärvi data set. Besides these two special cases of absorption in the E- and F-regions, we also note that EISCAT routinely monitors the plasma state of the whole ionosphere up to at least several hundred km altitude. The radar system thus provides information for a wide range of possible studies using ground-based instruments, of which EISCAT and IRIS are but two.

3.8. *Ionospheric modification*

All the foregoing topics concerned natural geophysical phenomena. The EISCAT facility also includes a powerful HF heating installation that has been used extensively to modify the ionospheric plasma, often with simultaneous radar measurements (Kohl *et al.*, 1993; Rietveld *et al.*, 1993). Two potential uses of IRIS in such experiments have recently been proposed. The first is the generation by the heater of small-scale electron density structures in the F-region (Honary *et al.*, 1996a). These should produce scintillations with particular properties in an IRIS beam that views the heated region when the line of sight is in the direction of a strong radio source such as Cassiopeia-A or Cygnus-A. (Natural scintillations, without heating, are regularly observed by IRIS. These are generally a nuisance for absorption studies and affected beams need to be excluded from image analysis. They do offer a method of studying natural small-scale structure in the F-region plasma, however.)

The second suggestion concerning combined heater and IRIS studies is the possible generation of energetic electrons when heating at a pump frequency close to an electron gyro-harmonic (Honary *et al.*, 1996b). These electrons might precipitate and produce absorption in the IRIS beam observing the D-region on the same field line as the heated F-region. This area of study is just developing and, in common with other applications of IRIS, new results are expected.

4. SUMMARY

The overlapping fields-of-view of the EISCAT incoherent scatter radar system and the Kilpisjärvi IRIS facility complement each other in providing both spatial (horizontal and vertical) and temporal information on auroral disturbances. The IRIS data define the spatial extent and dynamics of energetic precipitation events that EISCAT probes with one, or two, pencil beams. D-region electron density and spectral width are the prime parameters for combined studies, though observations of winds, electric fields and upper ionosphere quantities are also relevant. Interpretation of spectral width measurements in terms of aeronomical quantities using ion-chemical models will be an important next step in such studies.

In the present article, the main aspects of EISCAT and IRIS data have been introduced briefly with the intention of illustrating the variety of topics that may be investigated using such observations. The main results of this initial comparison illustrate many similarities with optical observations of visible aurora, and it is clear that the inclusion of such data in future studies will be a valuable complement.

While studies of many of the phenomena described above may be addressed using EISCAT CP data (with 5 or 10 s resolution), the examination of very dynamic events may require special radar experiments with better time resolution.

An exciting prospect for the near future, as the

activity of solar cycle 23 picks up, is simultaneous observations by EISCAT and IRIS during solar proton events. Detailed comparisons should offer new insight into both mesospheric ion chemistry and magnetospheric conditions during such events.

Information on the very different ionospheric properties that can cause radio absorption in the D-, E- and F-regions is readily available from the radar. Such observations will also be useful in conjunction with IRIS during experiments using the EISCAT heating facility.

Finally, we note that the IRIS data will enable more accurate synoptic investigations between radar and riometer because of the much smaller spatial integration of absorption compared with a standard riometer. One such example is the calibration of the riometer in terms of electron density at a given height for a particular magnitude, and possibly type, of absorption event.

Acknowledgements—We appreciate the co-operation of H. Ranta and A. Ranta (Sodankylä Geophysical Observatory) with logistical support for the IRIS facility at Kilpisjärvi, as well as for discussions regarding the data. S. Browne (University of Lancaster) was responsible for the reduction of the IRIS data. The Kilpisjärvi IRIS was constructed and is operated with funding from the UK Particle Physics and Astronomy Research Council. EISCAT is a joint European project supported by Suomen Akatemia of Finland, Centre National de la Recherche Scientifique of France, Max-Planck-Gesellschaft of Germany, Norges Forskningsråd of Norway, Naturvetenskapliga Forskningsrådet of Sweden and the Particle Physics and Astronomy Research Council of the United Kingdom.

REFERENCES

Aikio A. T. and Kaila K. U. 1996 A substorm observed by EISCAT and other ground-based instruments - evidence for near-Earth substorm initiation. *J. atmos. terr. Phys.* **58,** 5–21.

Burns C. J., Turunen E., Matveinen H., Ranta H. and Hargreaves J. K. 1991 Chemical modelling of the quiet summer D- and E-regions using EISCAT electron density profiles. *J. atmos. terr. Phys.* **53,** 115–134.

Collis P. N., Hargreaves J. K. and White G. P. 1996 A localised co-rotating auroral absorption event observed near local noon using imaging riometer and EISCAT, Ann. Geophys. **14,** 1305–1316.

Collis P. N. and Röttger J. 1990 Mesospheric studies using the EISCAT UHF and VHF radars: a review of principles and experimental results. *J. atmos. terr. Phys.* **52,** 569–584.

Collis P. N. and Rietveld M. T. 1990 Mesospheric observations with the EISCAT UHF radar during polar cap absorption events: 1. Electron densities and negative ions. *Ann. Geophys.* **8,** 809–824.

Collis P. N. and Korth A. 1983 Auroral radio absorption and the westward travelling surge. *Planet. Space Sci.* **31,** 1373–1378.

Collis P. N., Hargreaves J. K. and Korth A. 1984 Auroral radio absorption as an indicator of magnetospheric electrons and of conditions in the disturbed auroral D-region. *J. atmos. terr. Phys.* **46,** 21–38.

Detrick D. L. and Rosenberg T. J. 1990 A phased array radiowave imager for studies of cosmic noise absorption. *Radio Sci.* **25,** 325–338.

Evans J. V. 1969 Theory and practice of ionosphere study by Thomson scatter radar. *Proc. I.E.E.E.* **57,** 496–530.

Folkestad K., Hagfors T. and Westerlund S. 1983 EISCAT: an updated description of technical characteristics and operational capabilities. *Radio Sci.* **18,** 867–879.

Hargreaves J. K. 1980 D-region electron densities observed by incoherent-scatter radar during auroral-absorption spike events. *J. atmos. terr. Phys.* **42,** 783–789.

Hargreaves J. K. 1969 Auroral absorption of HF radio waves in the ionosphere: a review of results from the first decade of riometry, *Proc. I.E.E.E.*, **57(8),** 1348–1373.

Hargreaves J. K. and Devlin T. 1990 Morning sector electron precipitation events observed by incoherent scatter radar. *J. atmos. terr. Phys.* **52,** 193–203.

Hargreaves J. K., Shirochkov A. V. and Farmer A. D. 1993 The polar cap absorption event of 19-21 March 1990: recombination coefficients, the twilight transition and the midday recovery. *J. atmos. terr. Phys* **55,** 857–862

Hargreaves J. K., Browne S., Ranta H., Ranta A., Rosenberg T. J. and Detrick D. L. 1997 A study of substorm-associated nightside spike events in auroral absorption using imaging riometers at South Pole and Kilpisjärvi, *J. atmos. sol.-terr. Phys*, **59**, 853–872 (this issue).

Honary F., Browne S. and Rietveld M. T. 1995a Observation of heater-induced scintillation by an imaging riometer, paper presented at the 7th EISCAT Workshop, Cargèse, Corsica, 2–6 October, 1995.

Honary F., Stocker A. J., Rietveld M. T., McCrea I. and Browne S. 1995b Heater-induced effects on incoherent scatter spectra for pump frequencies close to the third harmonic of the electron gyro-frequency, paper presented at the 7th EISCAT Workshop, Cargèse, Corsica, 2–6 October, 1995.

Kauristie K., Pulkkinen T. I., Pellinen R. J., Janhunen P., Huuskonen A., Viljanen A., Opgenoorth H. J., Heikkila W. J. and Baker D. N. 1995 Analysis of the substorm trigger phase using multiple ground-based instrumentation. *Geophys. Res. Lett.* **22**, 2065–2068.

Kikuchi T., Yamagishi H. and Sato N. 1988 Eastward propagation of CNA pulsations of Pc 4–5 periods in the morning sector observed with scanning narrow beam riometer at L = 6.1. *Geophys. Res. Lett.* **15**, 168–171.

Kohl H., Kopka H., Stubbe P. and Rietveld M. T. 1993 Introduction to ionospheric heating at Tromsø—II. Scientific problems. *J. atmos. terr. Phys.* **55**, 601–613.

Lanchester B. S., Palmer J. R., Rees M. H., Lummerzheim D., Kaila K. and Turunen T. 1994 Energy flux and characteristic energy of an elemental auroral structure. *Geophys. Res. Lett.* **21**, 2789–2792.

Mathews J. D. 1986 Incoherent scatter radar probing of the 60–100 km atmosphere and ionosphere. *I.E.E.E. Trans. Geosci. Remote Sensing GE-* **24**, 765–776.

Nielsen E. 1980 Dynamics and spatial scale of auroral absorption spikes associated with the substorm expansion phase. *J. geophys. Res.* **85**, 2092–2098.

Nielsen E. and Axford W. I. 1977 Small scale auroral absorption events associated with substorms. *Nature* **267**, 502–504.

Opgenoorth H. J., Häggström I., Williams P. J. S. and Jones G. O. L. 1990 Regions of strongly enhanced perpendicular electric field adjacent to auroral arcs. *J. atmos. terr. Phys.* **52**, 449–458.

Ranta H., Yamagishi H. and Stauning P. 1995 Twilight anomaly, midday recovery and cutoff latitudes during the intense polar cap absorption event of March 1991. *Ann. Geophys.* **13**, 262–276.

Rietveld M. T. and Collis P. N. 1993 Mesospheric observations with the EISCAT UHF radar during polar cap absorption events: 2. Spectral measurements. *Ann. Geophys.* **11**, 797–808.

Rietveld M. T., Kohl H., Kopka H., Stubbe P. and Rietveld M. T. 1993 Introduction to ionospheric heating at Tromsø—I. Experimental overview. *J. atmos. terr. Phys.* **55**, 577–599.

Rishbeth H. and van Eyken A. P. 1993 EISCAT: early history and the first ten years of operation. *J. atmos. terr. Phys.* **55**, 525–542.

Rosenberg T. J., Wang Z., Rodger A. S., Dudeney J. R. and Baker K. B. 1993 Imaging riometer and H.F. radar measurements of drifting F region electron density structures in the polar cap. *J. geophys. Res.* **98**, 7757–7764.

Röttger J. 1994 Solar proton events: a source for long period gravity waves in the polar mesosphere?, Proc. STEP Symp., 1992, Laurel, Maryland, USA, 473–476.

Stauning P. 1984 Absorption of cosmic noise in the E-region during electron heating events. A new class of riometer absorption events. *Geophys. Res. Lett.* **11**, 1184–1187.

Turunen E. 1993 EISCAT incoherent scatter radar observations and model studies of day to twilight variations in the D-region during the PCA event of August, 1989. *J. atmos. terr. Phys.* **55**, 767–781.

Turunen T. 1986 GEN-SYSTEM—a new experimental philosophy for EISCAT radars. *J. atmos. terr. Phys.* **48**, 777–785.

Wang Z., Rosenberg T. J., Stauning P., Basu S. and Crowley G. 1994 Calculations of riometer absorption associated with F region plasma structures based on Søndre Strømfjord incoherent scatter radar observations. *Radio Sci.* **29**, 209–215.